Forster Resonance Energy Transfer Studies of Luminescent Gold Nanoparticles Functionalized with Ruthenium(II) and Rhenium(I) Complexes: Modulation via Esterase Hydrolysis

ARTICLE *in* ACS APPLIED MATERIALS & INTERFACES · APRIL 2014

Impact Factor: 6.72 · DOI: 10.1021/am500350c · Source: PubMed

ORGANOMETALLICS

Article

Synthesis of Coumarin-Appended Pyridyl Tricarbonylrhenium(I) 2,2#-Bipyridyl Complexes with Oligoether Spacer and Their Fluorescence Resonance Energy Transfer Studies

Mei-Jin Li, Wai-Ming Kwok, Wai Han Lam, Chi-Hang Tao, Vivian Wing-Wah Yam, and David Lee Phillips

Organometallics, **2009**, 28 (6), 1620-1630• DOI: 10.1021/om8006486 • Publication Date (Web): 27 February 2009

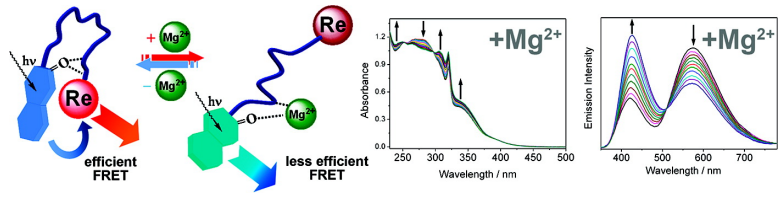

More About This Article

Additional resources and features associated with this article are available within the HTML version:

- Supporting Information
- Access to high resolution figures
- Links to articles and content related to this article
- Copyright permission to reproduce figures and/or text from this article

View the Full Text HTML

Articles

Synthesis of Coumarin-Appended Pyridyl Tricarbonylrhenium(I) 2,2′-Bipyridyl Complexes with Oligoether Spacer and Their Fluorescence Resonance Energy Transfer Studies

Mei-Jin Li, Wai-Ming Kwok,† Wai Han Lam, Chi-Hang Tao, Vivian Wing-Wah Yam,* and David Lee Phillips

Department of Chemistry, The University of Hong Kong, Pokfulam Road, Hong Kong SAR, People's Republic of China

Received July 9, 2008

A series of rhenium(I) complexes with appended coumarin ligand has been synthesized and characterized, and their fluorescence resonance energy transfer (FRET) properties have been studied. The interaction of the complexes with metal ions was investigated by UV−vis, luminescence, and NMR spectroscopic methods. The binding of various metal ions of different sizes would cause the changes in the conformation of the molecule, leading to a change in the donor−acceptor distance and FRET efficiency.

Introduction

Photoinduced energy transfer is a photoprocess of paramount importance and is currently being exploited for various applications such as in molecular and supramolecular photophysics,[1] polymer physics,[2] biology,[3] energy harvesting, and molecular devices.[4] Suitable combinations of donor−acceptor organic/inorganic materials can be employed to efficiently tune the emission toward different parts of the UV−visible−NIR region. The Förster-type energy transfer mechanism was proposed by Förster in 1948.[5] When the energy transfer was between two fluorophores, it could also be called fluorescence resonance energy transfer (FRET). FRET is a photophysical phenomenon where energy that is absorbed by one fluorescent molecule (donor) is transferred nonradiatively to a second fluorescent molecule (acceptor). The efficiency of FRET depends on the spectral overlap of the donor emission spectrum and the acceptor absorption spectrum, the orientation of the chromophores, and their distance and typically decreases rapidly beyond ∼100 Å.

Systems of particular interest are bichromophoric molecules containing a donor capable of transferring its excitation energy to an acceptor linked to it by a spacer. Such supramolecules are well suited for the study of fundamental aspects of excitation energy transfer and for applications as laser dyes, frequency converters of light, molecular devices, and molecular sensors. Because this process is distance and orientation dependent, the rate of transfer can be modified by inducing changes in the mutual distance and orientation of the donor and acceptor moieties by means of an external perturbation acting on the spacer. These kinds of systems usually show large Stokes shifts and are potentially useful for chemosensing or biosensing applicaitons.

Although there are a number of reports based on FRET,[1,3] most of them are confined to systems containing two organic chromophores requiring relatively short wavelength and high-energy excitation sources, and sensitivity still remains an issue. To increase the sensitivity, lanthanide complexes, especially those of europium(III) and terbium(III),[6] have been reported to be one kind of suitable candidates due to their strong luminescence and long excited-state lifetimes of up to millisecond range, which can be readily measured in a time-resolved mode.

* Corresponding author. E-mail: wwyam@hku.hk.
† Present address: Department of Applied Biology and Chemical Technology, Hong Kong Polytechnic University, Kowloon, Hong Kong SAR, People's Republic of China.

(1) (a) Valeur, B.; Pouget, J.; Bourson, J.; Kaschke, M.; Ernsting, N. P. *J. Phys. Chem.* **1992**, *96*, 6545. (b) Hoeben, F. J. M.; Shklyarevskiy, I. O.; Pouderoijen, M. J.; Engelkamp, H.; Schenning, A. P. H. J.; Christianen, P. C. M.; Maan, J. C.; Meijer, E. W. *Angew. Chem., Int. Ed.* **2006**, *45*, 1232.

(2) (a) Schultze, X.; Serin, J.; Adronov, A.; Frechet, J. M. J. *Chem. Commun.* **2001**, 1160. (b) Serin, J.; Schultze, X.; Adronov, A.; Frechet, J. M. J. *Macromolecules* **2002**, *35*, 5396.

(3) (a) Oh, E.; Hong, M. Y.; Lee, D.; Nam, S. H.; Yoon, H. C.; Kim, H. S. *J. Am. Chem. Soc.* **2005**, *127*, 3270. (b) Takakusa, H.; Kikuchi, K.; Urano, Y.; Sakamoto, S.; Yamaguchi, K.; Nagano, T. *J. Am. Chem. Soc.* **2002**, *124*, 1653. (c) Miyawaki, A.; Llopis, J.; Heim, R.; McCaffery, J. M.; Adams, J. A.; Ikura, M.; Tsien, R. Y. *Nature* **1997**, *388*, 882. (d) Zlokarnik, G.; Negulescu, P. A.; Knapp, T. E.; Mere, L.; Burres, N.; Feng, L.; Whitney, M.; Roemer, K.; Tsien, R. Y. *Science* **1998**, *279*, 84. (e) Mochizuki, N.; Yamashita, S.; Kurokawa, K.; Ohba, Y.; Nagai, T.; Miyawaki, A.; Matsuda, M. *Nature* **2001**, *411*, 1065. (f) Hanaoka, K.; Kikuchi, K.; Kojima, H.; Urano, Y.; Nagano, T. *J. Am. Chem. Soc.* **2004**, *126*, 12470.

(4) (a) Noh, Y. Y.; Lee, C. L.; Kim, J. J. *J. Chem. Phys.* **2003**, *118*, 2853. (b) Hong, X.; Zhang, C.; Liu, X.; Qiu, S.; Lu, P.; Shen, F.; Zhang, J.; Ma, Y. *J. Phys. Chem. B* **2004**, *108*, 3185. (c) Baldo, M. A.; Forrest, S. R. *Phys. Rev. B* **2000**, *62*, 10958. (d) Clcavc, V.; Yahioglu, G.; Lc Barny, P.; Friend, R. H.; Tesslcr, N. *Adv. Mater.* **1999**, *11*, 285. (e) Belser, P.; De Cola, L.; Hartl, F.; Adamo, V.; Bozic, B.; Chriqui, Y.; Mahadevan Iyer, V.; Jukes, R. T. F.; Kühni, J.; Querol, M.; Roma, S.; Salluce, N. *Adv. Funct. Mater.* **2006**, *16*, 195.

(5) Förster, T. *Ann. Phys.* **1948**, *2*, 55.

(6) (a) Alpha, B.; Lehn, J.-M.; Mathis, G. *Angew. Chem., Int. Ed. Engl.* **1987**, *26*, 266. (b) Alpha, B.; Balzani, V.; Lehn, J.-M.; Perathoner, S.; Sabbatini, N. *Angew. Chem., Int. Ed. Engl.* **1987**, *26*, 1266. (c) Tremblay, M. S.; Halim, M.; Sames, D. *J. Am. Chem. Soc.* **2007**, *129*, 7570. (d) Kupcho, K. R.; Stafslien, D. K.; DeRosier, T.; Hallis, T. M.; Ozers, M. S.; Vogel, K. W. *J. Am. Chem. Soc.* **2007**, *129*, 13372. (e) Barnhill, H. N.; Claudel-Gillet, S.; Ziessel, R.; Charbonniere, L. J.; Wang, Q. *J. Am. Chem. Soc.* **2007**, *129*, 7799.

10.1021/om8006486 CCC: $40.75
Publication on Web 02/27/2009

Scheme 1. Synthetic Routes for the Target Ligands and Complexes

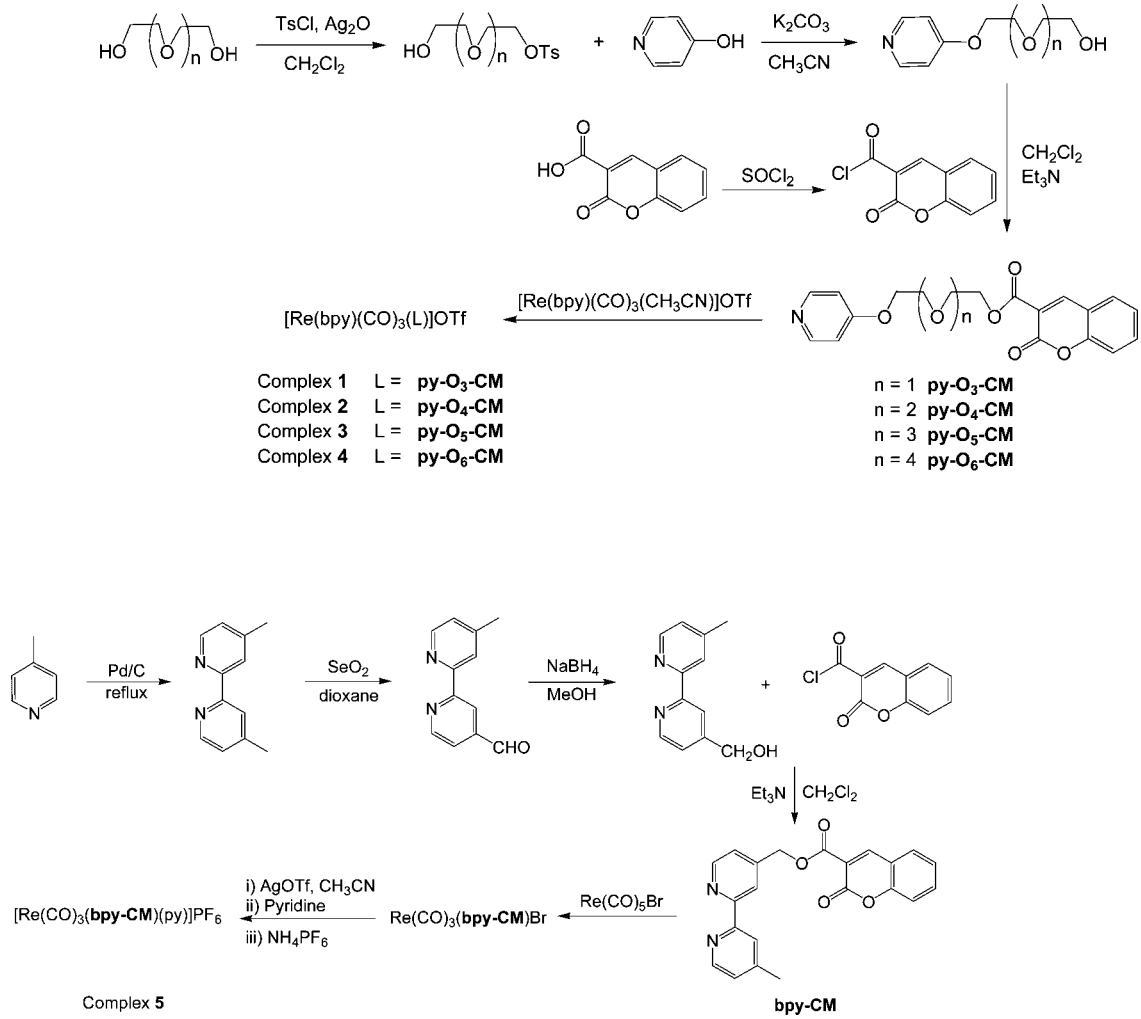

However, one major drawback is their relatively low stability, resulting in dissociation at low concentrations, which can be overcome by the introduction of more sophisticated encapsulating ligands. On the contrary, d block transition metal complexes are relatively less explored despite the rich photophysical behavior and high stability of a number of late transition metal complexes. Of the late transition metal complex systems, d^6 transition metal polypyridine complexes, especially that of ruthenium(II) and rhenium(I),[7] are the most widely studied systems due to the presence of MLCT bands in the visible region, versatile and easy preparation procedure, high photostability and luminescence quantum efficiency, and long-lived triplet excited state. Recently, there has been a growing interest in the study of FRET systems involving metal polypyridine complexes, especially that of ruthenium(II).[4e,8] Ruthenium(II) complexes as alternative energy transfer acceptor units for light-harvesting dyes or protease assay have been reported.[2,9] In this work, attempts have been made to focus on the design and synthesis of rhenium(I) complexes for FRET-based sensors due to their thermodynamic stability, chemical inertness, straightforward synthetic accessibility, and their relatively long-lived excited states. In this Article, several rhenium(I) complexes with oligoether-appended coumarin ligands, [Re(CO)$_3$(bpy)(**py-O$_3$-CM**)]OTf (**1**), [Re(CO)$_3$(bpy)(**py-O$_4$-CM**)]OTf (**2**), [Re(CO)$_3$(bpy)(**py-O$_5$-CM**)]OTf (**3**), [Re(CO)$_3$(bpy)(**py-O$_6$-CM**)]OTf (**4**), and [Re(CO)$_3$(py)(**bpy-CM**)]PF$_6$ (**5**) (Scheme 1), which might serve as FRET-based sensors for metal ions, have been synthesized and characterized, and their photophysical properties were studied. The interaction of the complexes with metal ions was investigated by UV−vis, luminescence, and NMR spec-

(7) (a) Bradley, P. G.; Kress, N.; Hornberger, B. A.; Dallinger, R. F.; Woodruff, W. H. *J. Am. Chem. Soc.* **1981**, *103*, 7441. (b) Smothers, W. K.; Wrighton, M. S. *J. Am. Chem. Soc.* **1983**, *105*, 1067. (c) Caspar, J. V.; Westmoreland, T. D.; Allen, G. H.; Bradley, P. G.; Meyer, T. J.; Woodruff, W. H. *J. Am. Chem. Soc.* **1984**, *106*, 3492. (d) Durham, B.; Caspar, J. V.; Nagle, J. K.; Meyer, T. J. *J. Am. Chem. Soc.* **1982**, *104*, 4803. (e) Ward, M. D.; Barigelletti, F. *Coord. Chem. Rev.* **2001**, *216*, 127. (f) Charbonniere, L. J.; Ziessel, R. F.; Sams, C. A.; Harriman, A. *Inorg. Chem.* **2003**, *42*, 3466. (g) Caspar, J. V.; Sullivan, B. P.; Meyer, T. J. *Inorg. Chem.* **1984**, *23*, 2104. (h) Caspar, J. V.; Meyer, T. J. *J. Phys. Chem.* **1983**, *87*, 952. (i) Yam, V. W. W.; Wong, K. M. C.; Lee, V. W. M.; Lo, K. K. W.; Cheung, K. K. *Organometallics* **1995**, *14*, 4034. (j) Uppadine, L. H.; Redman, J. E.; Dent, S. W.; Drew, M. G. B.; Beer, P. D. *Inorg. Chem.* **2001**, *40*, 2860. (k) Sun, S. S.; Lee, A. J.; Zavalij, P. Y. *Inorg. Chem.* **2003**, *42*, 3445. (l) Stoeffler, H. D.; Thornton, N. B.; Temkin, S. L.; Schanze, K. S. *J. Am. Chem. Soc.* **1995**, *117*, 7119. (m) Walters, K. A.; Premvardhan, L. L.; Peteanu, L. A.; Schanze, K. S. *Chem. Phys. Lett.* **2001**, *339*, 3. (n) Sun, S. S.; Lees, A. J. *J. Am. Chem. Soc.* **2000**, *122*, 8956. (o) Lewis, J. D.; Bussotti, L.; Foggi, P.; Perutz, R. N.; Moore, J. N. *J. Phys. Chem. A* **2002**, *106*, 12202. (p) Lewis, J. D.; Perutz, R. N.; Moore, J. N. *Chem. Commun.* **2000**, 1865.

(8) (a) Tyson, D. S.; Castellano, F. N. *Inorg. Chem.* **1999**, *38*, 4382. (b) Haider, J. M.; Williams, R. M.; De Cola, L.; Pikramenou, Z. *Angew. Chem., Int. Ed.* **2003**, *42*, 1830. (c) Welter, S.; Salluce, N.; Belser, P.; Groeneveld, M.; De Cola, L. *Coord. Chem. Rev.* **2005**, *249*, 1360. (d) Dupray, L. M.; Devenney, M.; Striplin, D. R.; Meyer, T. J. *J. Am. Chem. Soc.* **1997**, *119*, 10243. (e) Hurley, D. J.; Tor, Y. *J. Am. Chem. Soc.* **2002**, *124*, 13231.

(9) Kainmuller, E. K.; Olle, E. P.; Bannwarth, W. *Chem. Commun.* **2005**, 5459.

troscopic methods, and the binding constants of the complexes for metal ions were determined.

Experimental Section

Materials and Reagents. Rhenium(I) pentacarbonyl bromide, thionyl chloride, and silver trifluoromethanesulfonate were purchased from Aldrich Chemical Co. Diethylene glycol, triethylene glycol, tetraethylene glycol, pentaethylene glycol, *p*-toluenesulfonyl chloride, 4-hydroxypyridine, coumarin-3-carboxylic acid, and anhydrous potassium carbonate were all of analytical grade and were purchased from Lancaster Synthesis Ltd. Tetra-*n*-butylammonium perchlorate, magnesium(II) perchlorate, calcium(II) perchlorate tetrahydrate, barium(II) perchlorate, lithium perchlorate, sodium perchlorate, potassium perchlorate, and lead(II) perchlorate hydrate were purchased from Aldrich Chemical Co. with purity over 99.0%. Diethylene glycol monotosylate,[10] triethylene glycol monotosylate,[10] tetraethylene glycol monotosylate,[10] pentaethylene glycol monotosylate,[10] and 4-methyl-4′-hydroxymethyl-2,2′-bipyridine[11] were synthesized according to the literature methods.

Caution: Metal perchlorate salts are potentially explosive. Only small amounts of these materials should be handled and with great caution.

Synthesis. 1-(4-Pyridyloxy)-3-oxapentane-5-ol. It was prepared by modification of a literature method for a related phenyl oligoether.[12] A mixture of 4-hydroxypyridine (0.19 g, 2.0 mmol), diethylene glycol monotosylate (0.52 g, 2.0 mmol), and K_2CO_3 (0.55 g, 4.0 mmol) in dry MeCN (30 mL) was heated to reflux for 24 h with stirring under nitrogen. The mixture was cooled to room temperature, and the solvent was removed in vacuo. Deionized water (20 mL) was added to the mixture, and the solution was extracted three times with CH_2Cl_2. The combined extracts were dried over anhydrous Na_2SO_4, filtered, and evaporated to dryness. The residue was column chromatographed on silica gel with $CHCl_3$−MeOH (20:1, v/v) as the eluent to give the product as a colorless oil. Yield: 0.27 g, 75%. ^{1}H NMR ($CDCl_3$): δ 3.54 (m, 2H, CH_2O), 3.65 (m, 2H, CH_2O), 3.74 (t, J = 4.6 Hz, 2H, CH_2O), 4.03 (t, J = 4.6 Hz, 2H, CH_2O), 6.68 (dd, J = 4.8, 1.5 Hz; 2H, pyridyl H), 8.25 (dd, J = 4.8, 1.5 Hz; 2H, pyridyl H). Positive EI-MS: m/z 184 (M^+).

1-(4-Pyridyloxy)-3,6-dioxaoctane-8-ol. The procedure was similar to that described for the synthesis of 1-(4-pyridyloxy)-3-oxapentane-5-ol. Yield: 0.35 g, 78%. ^{1}H NMR ($CDCl_3$): δ 3.64 (m, 2H, CH_2O), 3.72 (m, 6H, CH_2O), 3.88 (t, J = 4.5 Hz, 2H, CH_2O), 4.18 (t, J = 4.5 Hz, 2H, CH_2O), 6.83 (dd, J = 5.1, 1.5 Hz; 2H, pyridyl H), 8.42 (dd, J = 5.1, 1.5 Hz; 2H, pyridyl H). Positive EI-MS: m/z 228 (M^+).

1-(4-Pyridyloxy)-3,6,9-trioxaundecane-11-ol. The procedure was similar to that described for the synthesis of 1-(4-pyridyloxy)-3-oxapentane-5-ol. Yield: 0.43 g, 80%. ^{1}H NMR ($CDCl_3$): δ 3.61 (m, 2H, CH_2O), 3.68 (m, 6H, CH_2O), 3.72 (m, 4H, CH_2O), 3.89 (t, J = 4.6 Hz, 2H, CH_2O), 4.19 (t, J = 4.6 Hz, 2H, CH_2O), 6.84 (dd, J = 4.9, 1.5 Hz; 2H, pyridyl H), 8.41 (dd, J = 4.9, 1.5 Hz; 2H, pyridyl H). Positive EI-MS: m/z 272 (M^+).

1-(4-Pyridyloxy)-3,6,9,12-tetraoxatetradecane-14-ol. The procedure was similar to that described for the synthesis of 1-(4-pyridyloxy)-3,6,9-trioxaundecane-11-ol, except that pentaethylene glycol monotosylate (0.79 g, 2mmol) was used instead of tetraethylene glycol monotosylate. Yield: 0.54 g, 85%. ^{1}H NMR ($CDCl_3$): δ 3.60 (m, 2H, CH_2O), 3.66 (m, 10H, CH_2O), 3.72 (m, 4H, CH_2O), 3.87 (t, J = 4.6 Hz, 2H, CH_2O), 4.18 (t, J = 4.6 Hz, 2H, CH_2O), 6.84 (dd, J = 4.8, 1.5 Hz; 2H, pyridyl H), 8.41 (dd, J = 4.8, 1.5 Hz; 2H, pyridyl H). Positive EI-MS: m/z 316 (M^+).

Coumarin-3-carboxylic Acid 1-(4-Pyridyloxy)-3-oxapentane-5-yl Ester (py-O$_3$-CM). Py-O$_3$-CM was prepared by modification of a literature method for *p*-nitrophenyl-2,2′-bipyridine-4,4′-dicarboxylate.[13] Coumarin-3-carboxylic acid (0.23 g, 1.2 mmol) was refluxed with thionyl chloride (3 mL) for 2 h to give a clear solution. The excess of thionyl chloride was removed by distillation, and the residue was dried in vacuum. The white solid residue was then dissolved in dry CH_2Cl_2 (5 mL), and this was added dropwise to the solution of 1-(4-pyridyloxy)-3-oxapentane-5-ol (0.18 g, 1 mmol) with Et_3N (0.2 mL) in dry CH_2Cl_2 (10 mL) at 0 °C. The mixture was heated to reflux overnight after the addition was complete. The mixture was cooled to room temperature, and the solvent was removed in vacuo. The residue was then column chromatographed on silica gel with $CHCl_3$ as the eluent to give **py-O$_3$-CM** as a white solid. Yield: 0.25 g, 70%. ^{1}H NMR ($CDCl_3$): δ 3.93 (m, 4H, CH_2O), 4.19 (t, J = 4.5 Hz, 2H, CH_2O), 4.53 (t, J = 4.5 Hz, 2H, CH_2O), 6.81 (d, J = 5.1 Hz, 2H, pyridyl H), 7.34 (m, 2H, coumarin H), 7.60 (m, 2H, coumarin H), 8.39 (d, J = 5.1 Hz, 2H, pyridyl H), 8.51 (s, 1H, coumarin H). Positive EI-MS: m/z 355 (M^+). Anal. Calcd for $C_{19}H_{17}NO_6$: C, 64.22; H, 4.82; N, 3.94. Found: C, 63.80; H, 4.78; N, 3.91.

Coumarin-3-carboxylic Acid 1-(4-Pyridyloxy)-3,6-dioxaoctane-8-yl Ester (py-O$_4$-CM). Py-O$_4$-CM was prepared by the procedure similar to that for the synthesis of **py-O$_3$-CM** and was isolated as a colorless oil. Yield: 0.32 g, 80%. ^{1}H NMR ($CDCl_3$): δ 3.75 (m, 4H, CH_2O), 3.88 (m, 4H, CH_2O), 4.17 (t, J = 4.7 Hz, 2H, CH_2O), 4.51 (t, J = 4.7 Hz, 2H, CH_2O), 6.80 (d, J = 4.8 Hz, 2H, pyridyl H), 7.34 (m, 2H, coumarin H), 7.60 (m, 2H, coumarin H), 8.39 (d, J = 4.8 Hz, 2H, pyridyl H), 8.55 (s, 1H, coumarin H). Positive EI-MS: m/z 399 (M^+). Anal. Calcd for $C_{21}H_{21}NO_7 \cdot 0.5H_2O$: C, 61.76; H, 5.43; N, 3.43. Found: C, 61.48; H, 5.41; N, 3.42.

Coumarin-3-carboxylic Acid 1-(4-Pyridyloxy)-3,6,9-trioxaundecane-11-yl Ester (py-O$_5$-CM). Py-O$_5$-CM was prepared by the procedure similar to that for the synthesis of **py-O$_3$-CM**. The residue was then column chromatographed on silica gel with $CHCl_3$ as the eluent to give **py-O$_5$-CM** as a colorless oil. Yield: 0.29 g, 65%. ^{1}H NMR ($CDCl_3$): δ 3.68 (m, 4H, CH_2O), 3.72 (m, 4H, CH_2O), 3.86 (m, 4H, CH_2O), 4.17 (t, J = 4.7 Hz, 2H, CH_2O), 4.50 (t, J = 4.7 Hz, 2H, CH_2O), 6.82 (d, J = 5.6 Hz, 2H, pyridyl H), 7.33 (m, 2H, coumarin H), 7.63 (m, 2H, coumarin H), 8.41 (d, J = 5.6 Hz, 2H, pyridyl H), 8.56 (s, 1H, coumarin H). Positive EI-MS: m/z 443 (M^+). Anal. Calcd for $C_{23}H_{25}NO_8 \cdot H_2O$: C, 59.86; H, 5.90; N, 3.04. Found: C, 60.35; H, 5.66; N, 3.13.

Coumarin-3-carboxylic Acid 1-(4-Pyridyloxy)-3,6,9,12-tetraoxatetradecane-14-yl Ester (py-O$_6$-CM). Py-O$_6$-CM was prepared by the procedure similar to that for the synthesis of **py-O$_3$-CM**, except 1-(4-pyridyloxy)-3,6,9,12-tetraoxatetradecane-14-ol (0.32 g, 1 mmol) was used instead of 1-(4-pyridyloxy)-3-trioxaundecane-5-ol. Chromatography on silica gel with $CHCl_3$ as the eluent gave **py-O$_6$-CM** as a colorless oil. Yield: 0.30 g, 61%. ^{1}H NMR ($CDCl_3$): δ 3.67 (m, 8H, CH_2O), 3.72 (m, 4H, CH_2O), 3.85 (m, 4H, CH_2O), 4.17 (t, J = 4.8 Hz, 2H, CH_2O), 4.50 (t, J = 4.8 Hz, 2H, CH_2O), 6.82 (dd, J = 5.6, 1.5 Hz, 2H, pyridyl H), 7.33 (m, 2H, coumarin H), 7.64 (m, 2H, coumarin H), 8.41 (dd, J = 5.6, 1.5 Hz, 2H, pyridyl H), 8.56 (s, 1H, coumarin H). Positive EI-MS: m/z 487 (M^+). Anal. Calcd for $C_{25}H_{29}NO_9 \cdot H_2O$: C, 60.48; H, 6.09; N, 2.82. Found: C, 59.82; H, 5.94; N, 3.09.

Coumarin-3-carboxylic Acid 4′-Methyl-[2,2′]bipyridinyl-4-ylmethyl Ester (bpy-CM). The procedure was similar to that for the synthesis of **py-O$_3$-CM**, except 4-methyl-4′-hydroxymethyl-2,2′-bipyridine (0.20 g, 1 mmol) was used instead of 1-(4-pyridyloxy)-3- trioxaundecane-5-ol. Chromatography on silica gel with $CHCl_3$ as the eluent gave **bpy-CM** as a white solid. Yield: 0.18 g, 48%. ^{1}H NMR ($CDCl_3$): δ 2.45 (s, 3H, CH_3), 5.50 (s, 2H, CH_2O), 7.15 (d, J = 4.9 Hz, 1H, bipyridyl H), 7.36 (m, 2H,

(10) Bouzide, A.; Sauve, G. *Org. Lett.* **2002**, *4*, 2329.
(11) Farah, A. A.; Pietro, W. J. *Can. J. Chem.* **2004**, *82*, 595.
(12) Van Staveren, C. J.; Reinhoudt, D. N.; Van Eerden, J.; Harkema, S. *J. Chem. Soc., Chem. Commun.* **1987**, 974.
(13) Yagi, K.; Rivera-Castro, M. D. L.; Cedeno, R.; Inoue, M. *Inorg. Chim. Acta* **1987**, *131*, 273.

coumarin H), 7.49 (d, $J = 4.9$ Hz, 1H, bipyridyl H), 7.64 (m, 2H, coumarin H), 8.25 (s, 1H, bipyridyl H), 8.49 (s, 1H, bipyridyl H), 8.54 (d, $J = 4.9$ Hz, 1H, bipyridl H), 8.63 (s, 1H, coumarin H), 8.71 (d, $J = 4.9$ Hz, 1H, bipyridyl H). Positive EI-MS: *m*/*z* 373 (M^+). Anal. Calcd for $C_{22}H_{16}N_2O_4$: C, 70.96; H, 4.33; N, 7.52. Found: C, 70.85; H, 4.39; N, 7.40.

[Re(CO)$_3$(bpy)(py-O$_3$-CM)]OTf (1). The complex was synthesized according to a modification of a literature procedure for the related [Re(CO)$_3$(py)(bpy)]PF$_6$.[14] To a solution of [Re(CO)$_5$Br] (50 mg, 0.12 mmol) in benzene (15 mL) was added 2,2′-bipyridine (21 mg, 0.13 mmol), and the mixture was heated to reflux overnight under an inert atmosphere of nitrogen, during which the colorless solution turned yellow. After evaporation of the solvent, the residue was washed several times with diethyl ether and was then dissolved in CH_3CN (10 mL). To this solution was added AgOTf (38 mg, 0.15 mmol), and the mixture was heated to reflux in the dark overnight under nitrogen. The mixture was cooled to room temperature, followed by filtration of the insoluble AgBr to give a yellow solution. The solvent was removed in vacuo, and the yellow residue was dissolved in THF (10 mL). To this solution was added **py-O$_3$-CM** (53 mg, 0.15 mmol), and the mixture was heated to reflux overnight under nitrogen. After evaporation of the solvent, the residue was column chromatographed on silica gel with $CHCl_3$−acetone (v/v, 10:1) as the eluent to give the desired complex as the second yellow band. Subsequent recrystallization by vapor diffusion of diethyl ether into an acetonitrile solution of the complex afforded the desired complex as a yellow crystalline solid. Yield: 80 mg, 72%. ^{1}H NMR ($CDCl_3$): δ 3.82 (m, 4H, CH_2O), 4.18 (t, $J = 4.5$ Hz, 2H, CH_2O), 4.42 (t, $J = 4.5$ Hz, 2H, CH_2O), 6.85 (d, $J = 7.0$ Hz, 2H, pyridyl H), 7.35 (m, 2H, coumarin H), 7.65 (m, 2H, coumarin H), 7.77 (t, $J = 4.8$ Hz, 2H, bipyridyl H), 7.92 (d, $J = 7.0$ Hz, 2H, pyridyl H), 8.30 (t, $J = 8.2$ Hz, 2H, bipyridyl H), 8.55 (s, 1H, coumarin H), 8.68 (d, $J = 8.2$ Hz, 2H, bipyridyl H), 9.10 (d, $J = 4.8$ Hz, 2H, bipyridyl H). Positive FAB-MS: *m*/*z* 782 ([M − OTf]$^+$). IR (KBr disk, ν/cm^{-1}): 1909, 1919, 2030 ν (C≡O). Anal. Calcd for $C_{33}H_{25}F_3N_3O_{12}ReS \cdot H_2O$: C, 41.77; H, 2.87; N, 4.43. Found: C, 41.51; H, 2.93; N, 4.37.

[Re(CO)$_3$(bpy)(py-O$_4$-CM)]OTf (2). The procedure was similar to that described for the synthesis of [Re(CO)$_3$(bpy)(**py-O$_3$-CM**)]OTf, except **py-O$_4$-CM** (60 mg, 0.15 mmol) was used instead of **py-O$_3$-CM**. Recrystallization from CH_3CN−diethyl ether afforded the desired complex as a yellow crystalline solid. Yield: 75 mg, 64%. ^{1}H NMR ($CDCl_3$): δ 3.65 (m, 4H, CH_2O), 3.77 (m, 4H, CH_2O), 4.14 (t, $J = 4.6$ Hz, 2H, CH_2O), 4.43 (t, $J = 4.6$ Hz, 2H, CH_2O), 6.83 (d, $J = 7.1$ Hz, 2H, pyridyl H), 7.35 (m, 2H, coumarin H), 7.65 (m, 2H, coumarin H), 7.73 (t, $J = 4.8$ Hz, 2H, bipyridyl H), 7.88 (d, $J = 7.1$ Hz, 2H, pyridyl H), 8.32 (t, $J = 8.1$ Hz, 2H, bipyridyl H), 8.55 (s, 1H, coumarin H), 8.76 (d, $J = 8.1$ Hz, 2H, bipyridyl H), 9.06 (d, $J = 4.8$ Hz, 2H, bipyridyl H). Positive FAB-MS: *m*/*z* 826 ([M − OTf]$^+$). IR (KBr disk, ν/cm^{-1}): 1912, 1918, 2030 ν (C≡O). Anal. Calcd for $C_{35}H_{29}F_3N_3O_{13}ReS \cdot 2H_2O$: C, 41.58; H, 3.29; N, 4.16. Found: C, 41.64; H, 3.25; N, 3.87.

[Re(CO)$_3$(bpy)(py-O$_5$-CM)]OTf (3). The procedure was similar to that described for the synthesis of [Re(CO)$_3$(bpy)(**py-O$_3$-CM**)]PF$_6$, except **py-O$_5$-CM** (66 mg, 0.15 mmol) was used instead of **py-O$_3$-CM**. Recrystallization from CH_3CN−diethyl ether afforded the desired complex as a yellow crystalline solid. Yield: 81 mg, 67%. ^{1}H NMR ($CDCl_3$): δ 3.63 (m, 4H, CH_2O), 3.68 (m, 4H, CH_2O), 3.82 (m, 4H, CH_2O), 4.19 (t, $J = 4.6$ Hz, 2H, CH_2O), 4.50 (t, $J = 4.6$ Hz, 2H, CH_2O), 6.86 (d, $J = 7.1$ Hz, 2H, pyridyl H), 7.35 (m, 2H, coumarin H), 7.68 (m, 2H, coumarin H), 7.73 (t, $J = 4.9$ Hz, 2H, bipyridyl H), 7.86 (d, $J = 7.1$ Hz, 2H, pyridyl H), 8.29 (t, $J = 8.2$ Hz, 2H, bipyridyl H), 8.64 (s, 1H, coumarin H), 8.68 (d, $J = 8.2$ Hz, 2H, bipyridyl H), 9.07 (d, $J = 4.9$ Hz, 2H, bipyridyl H). Positive FAB-MS: *m*/*z* 870 ([M − OTf]$^+$). IR (KBr disk, ν/cm^{-1}): 1910, 1919, 2031 ν(C≡O). Anal. Calcd for $C_{37}H_{33}F_3N_3O_{14}ReS \cdot H_2O$: C, 42.86; H, 3.40; N, 4.05. Found: C, 42.71; H, 3.22; N, 3.96.

[Re(CO)$_3$(bpy)(py-O$_6$-CM)]OTf (4). This complex was synthesized according to a procedure similar to that described for the synthesis of complex **1**, except **py-O$_6$-CM** (73 mg, 0.15 mmol) was used instead of **py-O$_3$-CM**. Recrystallization from CH_3CN−diethyl ether gave complex as a yellow crystalline solid. Yield: 79 mg, 62%. ^{1}H NMR ($CDCl_3$): δ 3.58 (m, 10H, CH_2O), 3.63 (m, 2H, CH_2O), 3.68 (t, $J = 3.6$ Hz, 2H, CH_2O), 3.82 (t, $J = 3.6$ Hz, 2H, CH_2O), 4.12 (t, $J = 3.6$ Hz, 2H, CH_2O), 4.57 (t, $J = 3.6$ Hz, 2H, CH_2O), 6.83 (d, $J = 7.0$ Hz, 2H, pyridyl H), 7.34 (m, 2H, coumarin H), 7.66 (m, 2H, coumarin H), 7.78 (t, $J = 5.2$ Hz, 2H, bipyridyl H), 7.93 (d, $J = 7.0$ Hz, 2H, pyridyl H), 8.32 (t, $J = 8.0$ Hz, 2H, bipyridyl H), 8.58 (s, 1H, coumarin H), 8.74 (d, $J = 8.0$ Hz, 2H, bipyridyl H), 9.11 (d, $J = 5.2$ Hz, 2H, bipyridyl H). Positive FAB-MS: *m*/*z* 914 ([M − OTf]$^+$). IR (KBr disk, ν/cm^{-1}): 1912, 1920, 2031 ν(C≡O). Anal. Calcd for $C_{39}H_{37}F_3N_3O_{15}ReS \cdot H_2O$: C, 43.33; H, 3.63; N, 3.88. Found: C, 43.46; H, 3.52; N, 3.87.

[Re(CO)$_3$(py)(bpy-CM)]PF$_6$ (5). The complex was prepared according to modification of a literature method for the synthesis of [Re(CO)$_3$(py)(bpy)]PF$_6$.[14] To a solution of [Re(CO)$_5$Br] (50 mg, 0.12 mmol) in benzene (15 mL) was added **bpy-CM** (50 mg, 0.13 mmol), and the mixture was heated to reflux overnight under an inert atmosphere of nitrogen, during which the clear solution turned into a suspension. The mixture was cooled to room temperature and filtered to obtain the yellow solid. The solid was washed several times with CH_2Cl_2 and diethyl ether and was then suspended in CH_3CN (10 mL). To this mixture was added AgOTf (38 mg, 0.15 mmol), and the mixture was heated to reflux in the dark overnight under nitrogen. The mixture was cooled to room temperature, followed by filtration of the insoluble AgBr to give a clear yellow solution. The solvent was removed in vacuo, and the yellow residue was dissolved in THF (10 mL). To this solution was added pyridine (100 μL, 0.13 mmol), and the mixture was heated to reflux overnight under nitrogen. After removal of the solvent, the residue was dissolved in a minimum amount of water, and metathesis reaction upon addition of a saturated aqueous solution of NH_4PF_6 afforded the desired complex as a yellow solid, which was then obtained by filtration. Subsequent recrystallization by vapor diffusion of diethyl ether into an acetonitrile solution of the complex afforded [Re(CO)$_3$(py)(**bpy-CM**)]PF$_6$ as yellow needle-shaped crystals. ^{1}H NMR (CD_3CN): δ 2.57 (s, 3H, CH_3), 5.58 (s, 2H, CH_2O), 7.31 (t, $J = 8.6$ Hz, 2H, pyridyl H), 7.45 (m, 2H, coumarin H), 7.64 (d, $J = 5.7$ Hz, 1H, bipyridyl H), 7.74 (t, $J = 8.6$ Hz, 1H, pyridyl H), 7.81(m, 2H, coumarin H), 7.89 (d, $J = 5.7$, 1H, bipyridyl H), 8.26 (d, $J = 8.6$ Hz, 2H, pyridyl H), 8.31 (s, 1H, bipyridyl H), 8.59 (s, 1H, bipyridyl H), 8.77 (s, 1H, coumarin H), 9.05 (d, $J = 5.7$ Hz, 1H, bipyridyl H), 9.20 (d, $J = 5.7$, 1H, bipyridyl H). Positive FAB-MS: *m*/*z* 721 ([M − PF$_6$]$^+$). IR (KBr disk, ν/cm^{-1}): 1915, 1939, 2033 ν(C≡O). Anal. Calcd for $C_{30}H_{21}F_6N_3O_7PRe \cdot 0.5H_2O$: C, 41.15; H, 2.53; N, 4.80. Found: C, 41.10; H, 2.58; N, 4.66.

Physical Measurements and Instrumentation. Electronic absorption spectra were recorded on a Hewlett-Packard 8452A diode array spectrophotometer. Steady-state emission was recorded on a Spex Fluorolog-2 model F111 fluorescence spectrophotometer. ^{1}H NMR spectra were recorded on a Bruker DPX-300 or Bruker DPX-400 Fourier transform NMR spectrometer with chemical shifts reported relative to tetramethylsilane. ^{13}C NMR spectra, ^{1}H−^{13}C HETCOR, and HMBC two-dimensional spectra were recorded on a Bruker DPX-600 Fourier transform NMR spectrometer. Positive-ion FAB and EI mass spectra were recorded on a Finnigan MAT95 mass spectrometer. Elemental analysis of the complexes was performed on a Carlo Erba 1106 elemental analyzer at the Institute of Chemistry of the Chinese Academy of Sciences in Beijing. The transient absorption measurements were performed with a Ti:

(14) Sacksteder, L.; Zipp, A. P.; Brown, E. A.; Streich, J.; Demas, J. N.; DeGraff, B. A. *Inorg. Chem.* **1990**, *29*, 4335.

Sapphire regenerative amplified source operated at 1 mJ/pulse, 150 fs, 1 kHz, and 800 nm that has been described in detail elsewhere.[15]

Results and Discussion

Synthesis and Characterization. The synthetic routes for the ligands and complexes are summarized in Scheme 1. Conversion of coumarin 3-carboxylic acid to coumarin 3-carboxylic chloride was achieved via heating to reflux for 5 h in thionyl chloride. Monotosylates of tetraethylene glycol and pentaethylene glycol were prepared in high yield under neutral conditions in CH_2Cl_2 using a stoichiometric amount of *p*-toluenesulfonyl chloride in the presence of Ag_2O and a catalytic amount of KI according to the literature method.[10] The respective monotosylates were reacted with 4-hydroxypyridine in dry MeCN using K_2CO_3 as the base to give pyridine polyethylene glycols, followed by reaction with coumarin 3-carboxylic chloride to produce the desired ligands. The ligands and $[Re(bpy)(CO)_3(CH_3CN)]OTf$ were heated to reflux in THF overnight under N_2. Subsequent column chromatography on the silica gel and recrystallization from acetonitrile−diethyl ether gave the desired target complexes in reasonable yields. 4-Methyl-4′-hydroxymethyl-2,2′-bipyridine was prepared by the reported method using 4-picoline as the starting material,[11] followed by reaction with coumarin 3-carboxylic chloride to afford the ligand **bpy-CM**. $[Re(CO)_3(py)(\textbf{bpy-CM})]PF_6$ was produced by reaction of **bpy-CM** with $[Re(CO)_5Br]$ in benzene, followed by substitution of the bromo group with MeCN in the presence of AgOTf in MeCN, and the eventual replacement of MeCN by pyridine in THF, which was subsequently metathesized to the PF_6^- salt by the addition of a saturated aqueous solution of NH_4PF_6.

The identities of the ligands and the rhenium(I) complexes were confirmed by satisfactory ^1H NMR spectroscopy, EI or FAB mass spectrometry, and elemental analysis. The rhenium(I) complexes were also characterized by IR spectroscopy, which showed three strong stretches in the carbonyl region (1900−2100 cm^{-1}), typical of the facial arrangement of the three carbonyls in an octahedral geometry.[16]

Photophysical Properties. The electronic absorption spectra of the rhenium(I) complexes in acetonitrile solution showed intense absorption bands with molar extinction coefficients in the order of 10^4 dm^3 mol^{-1} cm^{-1} at ca. 250−340 nm, which were tentatively assigned as intraligand (IL) $\pi \rightarrow \pi^*$ transitions. The absorption bands with molar extinction coefficients in the order of 10^3 dm^3 mol^{-1} cm^{-1} at ca. 385 nm were ascribed to the $d\pi(Re) \rightarrow \pi^*(bpy)$ or $d\pi(Re) \rightarrow \pi^*(\textbf{bpy-CM})$ metal-to-ligand charge transfer (MLCT) transitions of the respective complexes, typical of rhenium(I) tricarbonyl diimine complex systems.[17] The electronic absorption data of the rhenium(I) complexes are summarized in Table 1.

Table 1. Electronic Absorption Data of the Re(I) Complexes in CH_3CN

complex	absorption λ_{abs}/nm (ε/dm^3 mol^{-1} cm^{-1})
1	252 (27 990), 282 (29 400), 320 (20 510), 340 (10 150), 385 (2490)
2	252 (27 070), 282 (30 840), 320 (18 830), 340 (9350), 385 (2270)
3	252 (25 400), 282 (26 520), 320 (18 840), 340 (9540), 385 (2430)
4	251 (24 650), 282 (25 640), 320 (17 970), 340 (9330), 385 (2650)
5	287 (28 500), 318 (20 950), 340 (12 420), 385 (2590)

The rhenium(I) complexes were found to show strong yellow emission upon excitation at room temperature in acetonitrile solution. The intense emission band with emission maximum at ca. 570 nm was attributed to ^{3}MLCT phosphorescence, similar to that observed in other related rhenium(I) complexes,[17] while the weaker blue emission band at ca. 420 nm was assigned as IL fluorescence of coumarin, similar to that observed in the free ligand. The ratios of the blue emission intensity (donor) at ca. 420 nm of complexes **1**−**4** to that of the yellow emission at ca. 570 nm (acceptor), I_D/I_A, were about 0.62, 0.58, 0.51, and 0.55, respectively, which may be indicative of a slight dependence of the energy transfer efficiency from the coumarin donor to the rhenium(I) complex acceptor being affected by the length of the oligoether spacer. However, this finding is not in line with that predicted from Förster theory,[18] in which the efficiency of energy transfer changes as a function of the inverse sixth power of the interchromophoric distance. In view of the flexibility of the oligoether linkage, the distance between the donor and the acceptor is not necessarily defined by the length of the oligoether spacer, and a conformation involving the folding of the flexible spacer that links the coumarin moiety and the Re(I) luminophore is possible, which gives rise to this anomalous observation. It is not unreasonable to envisage that the lengthening of the oligoether spacer would favor a folded conformation that brings the donor and acceptor moieties closer to each other due to the increase in degrees of freedom. This back-folding conformation may be further promoted by the presence of the carbonyl groups on the coumarin moiety with its propensity to form noncovalent interactions.[19] For complex **5**, in which the coumarin was directly linked to the bipyridine, the emission of coumarin was strongly quenched with an I_D/I_A ratio of ca. 0.05 observed. These results demonstrated that the length of the oligoether spacer, the type of linkage, and the conformation between the donor and the acceptor all play important roles in tuning the efficiency of the energy transfer.

Cation-Binding Properties. Electronic Absorption Studies. The cation-binding ability of complexes **1**−**4** was investigated by electronic absorption spectrophotometric method. Upon addition of metal ions such as alkali and alkaline earth metal ions to a solution of complexes **1**−**4** in CH_3CN (0.1 M $^nBu_4NClO_4$), spectral changes in the IL transition bands were observed. Upon addition of Li^+ and Na^+ ions to complexes **1**−**4** in acetonitrile, the small decrease of the band at about 280 nm

(15) (a) Ma, C.; Kwok, W. M.; Chan, W. S.; Du, Y.; Kan, J. T. W.; Toy, P. H.; Phillips, D. L. *J. Am. Chem. Soc.* **2006**, *128*, 2558. (b) Kwok, W. M.; Ma, C.; Phillips, D. L. *J. Am. Chem. Soc.* **2006**, *128*, 11894. (c) Ma, C.; Du, Y.; Kwok, W. M.; Phillips, D. L. *Chem.-Eur. J.* **2007**, *13*, 2290.

(16) Kaesz, H. D.; Bau, R.; Hendrickson, D.; Smith, J. M. *J. Am. Chem. Soc.* **1967**, *89*, 2844.

(17) (a) Hornaan, E.; Snow, M. R. *Aust. J. Chem.* **1980**, *33*, 2369. (b) Chen, P.; Curry, M.; Meyer, T. J. *Inorg. Chem.* **1989**, *28*, 2271. (c) Yam, V. W. W.; Lau, V. C. Y.; Cheung, K. K. *J. Chem. Soc., Chem. Commun.* **1995**, 259. (d) Yam, V. W. W.; Lau, V. C. Y.; Cheung, K. K. *Organometallics* **1996**, *15*, 1740. (e) Yam, V. W. W.; Wang, K. Z.; Wang, C. R.; Yang, Y.; Cheung, K. K. *Organometallics* **1998**, *17*, 2440. (f) Yam, V. W. W.; Chong, S. H. F.; Cheung, K. K. *Chem. Commun.* **1998**, 2121. (g) Yam, V. W. W.; Chong, S. H. F.; Ko, C. C.; Cheung, K. K. *Organometallics* **2000**, *19*, 5092.

(18) (a) Förster, T. *Z. Naturforsch., A: Phys. Sci.* **1949**, *4*, 319. (b) Förster, T. *Discuss. Faraday Soc.* **1959**, *27*, 7. (c) Stryer, L. *Annu. Rev. Biochem.* **1978**, *47*, 819. (d) Bourson, J.; Mugnier, J.; Valeur, B. *Chem. Phys. Lett.* **1982**, *92*, 430. (e) Mugnier, J.; Pouget, J.; Bourson, J.; Valeur, B. *J. Lumin.* **1985**, *33*, 273. (f) Valeur, B. In *Fluorescent Biomolecules, Methodologies and Applications*; Jameson, D. M., Reinhart, G. D., Eds.; Plenum: New York, 1989; p 269. (g) Valeur, B. In *Molecular Luminescence Spectroscopy, Part 3*; Schulman, S. G., Ed.; Wiley: New York, 1993; Vol. 77, Chapter 2.

(19) Density functional theory at the B3LYP level was used to optimize one of the possible folded conformations of **3** (for computational details, see the Supporting Information).

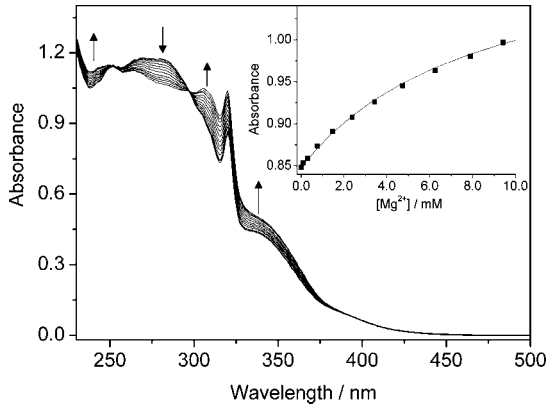

Figure 1. UV−vis spectral changes of $[Re(CO)_3(bpy)(\mathbf{py\text{-}O_5\text{-}CM})]^+$ (6.0×10^{-5} M) in CH_3CN (0.1 M ^{n}Bu$_4$NClO$_4$) upon addition of $Mg(ClO_4)_2$. The inset shows a plot of absorbance at 310 nm (■) as a function of $[Mg^{2+}]$ and its theoretical fit (−) according to a 1:1 binding model.

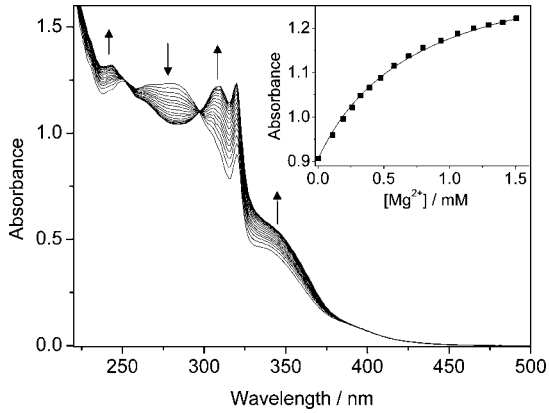

Figure 2. UV−vis spectral changes of $[Re(CO)_3(bpy)(\mathbf{py\text{-}O_6\text{-}CM})]^+$ (5.0×10^{-5} M) in CH_3CN (0.1 M ^{n}Bu$_4$NClO$_4$) upon addition of $Mg(ClO_4)_2$. The inset shows a plot of absorbance at 310 nm (■) as a function of $[Mg^{2+}]$ and its theoretical fit (−) according to a 1:1 binding model.

and the increase of the bands at about 320 and 340 nm produced a perfectly clean isosbestic point at ca. 295 nm. In the case of alkaline earth metal ions such as Mg^{2+}, Ca^{2+}, and Ba^{2+}, there were significant changes in the electronic absorption spectra, and two well-defined isosbestic points at ca. 252 and 297 nm were observed. The UV−visible spectral traces of complexes **3** and **4** upon addition of magnesium perchlorate are shown in Figures 1 and 2, respectively, and the insets show the plots of absorbance at 310 nm as a function of the added metal ion concentration and their theoretical fits according to a 1:1 binding model. With such information, the binding constants could be obtained by nonlinear least-squares fit[20] of the UV−vis absorbance versus the concentration of the added metal ions, and the titration data were found to show a good fit to that of a 1:1 binding model, confirming the 1:1 binding stoichiometry. The binding constants of complexes **1**−**4** for different metal ions are summarized in Table 2. The binding constants for K^+ and Cs^+ ions were not determined due to the low solubility of their perchlorate and hexafluorophosphate salts. There were no observable changes for the other transition metal ions such as Zn^{2+}, Cd^{2+}, and Hg^{2+}. In general, the binding affinities of complexes **1** and **2** for alkali metal ions were very low, and

(20) Bourson, J.; Pouget, J.; Valeur, B. *J. Phys. Chem.* **1993**, *97*, 4552.

Table 2. Binding Constants (log K_s) of Complexes 1−4 for Metal Ions in CH_3CN (0.1 M ^{n}Bu$_4$NClO$_4$)

	log K_s			
metal ion	**1**	**2**	**3**	**4**
Li^+	0.76 ± 0.01^a	0.80 ± 0.01^a	1.18 ± 0.01^a	1.76 ± 0.02^a
	$-^c$	$-^c$	1.38 ± 0.01^b	1.84 ± 0.01^b
Na^+	0.81 ± 0.01^a	0.95 ± 0.01^a	1.55 ± 0.01^a	2.03 ± 0.01^a
	$-^c$	$-^c$	$-^c$	2.01 ± 0.01^b
Mg^{2+}	1.78 ± 0.01^a	1.84 ± 0.01^a	2.15 ± 0.01^a	3.16 ± 0.01^a
	1.88 ± 0.01^b	1.87 ± 0.01^b	2.29 ± 0.01^b	3.13 ± 0.01^b
Ca^{2+}	2.28 ± 0.01^a	2.18 ± 0.01^a	2.52 ± 0.02^a	3.52 ± 0.02^a
	2.21 ± 0.01^b	2.24 ± 0.01^b	2.46 ± 0.01^b	3.35 ± 0.01^b
Ba^{2+}	1.70 ± 0.01^a	1.73 ± 0.01^a	2.63 ± 0.02^a	3.98 ± 0.02^a
	1.69 ± 0.02^b	1.85 ± 0.01^b	2.66 ± 0.01^b	3.73 ± 0.01^b
Pb^{2+}	1.93 ± 0.02^a	1.79 ± 0.01^a	3.29 ± 0.01^a	4.14 ± 0.05^a
	$-^c$	1.72 ± 0.02^b	3.03 ± 0.02^b	4.16 ± 0.04^b

[a] UV−visible spectrophotometric method. [b] Emission method. [c] The spectral changes were too small for an accurate determination of the binding constant.

those toward Ca^{2+} ions were the largest among the alkaline earth metal ions. On the other hand, the binding affinities of complexes **3** and **4** for various metal ions followed the order: $Pb^{2+} > Ba^{2+} > Ca^{2+} > Mg^{2+} >$ alkali metal ion. The larger binding constants for Ba^{2+} than Ca^{2+} in complexes **3** and **4** are in line with the longer oligoether spacers in **3** and **4** than in **1** and **2**, which better fit the larger Ba^{2+} ion. For the same metal ion, the binding constant was in the order of **4** > **3** > **2** ≈ **1**, revealing that, in general, the longer oligoether chain between the donor and the acceptor formed more stable complexes with the metal ions.

Emission Studies. The cation-binding ability of complexes **1**−**4** was also investigated by emission spectrophotometric studies. The emission spectral changes of complex **1** were insignificant upon addition of Li^+, Na^+, and Pb^{2+} ions and were too small for an accurate determination of binding constants. Similarly, the changes in the emission intensity of complex **2** were also too small to give an accurate determination of the binding constants after addition of Li^+ and Na^+ ions. Unlike complex **1**, addition of Pb^{2+} ions to complex **2** induced an obvious change in the emission spectra, probably due to the longer oligoether chain of complex **2**, and the binding constant was obtained according to the 1:1 binding model. The emission due to the coumarin donor in complexes **1** and **2** in acetonitrile (0.1 M ^{n}Bu$_4$NClO$_4$) showed a large increase in intensity, while the emission of the rhenium(I) complex acceptor was reduced in intensity upon addition of Mg^{2+} and Ca^{2+} ions, suggesting that binding of Mg^{2+} and Ca^{2+} ions would lead to a poorer FRET efficiency. On the contrary, the emission intensities of both the donor and the acceptor showed a slight increase upon addition of Ba^{2+} ions. The binding constants of complexes **1** and **2** toward different metal ions are summarized in Table 2, and the results showed that the Ca^{2+} ion gave the largest binding constants for complexes **1** and **2**, probably due to its better size fit into the cavity created by the oligoether chain.

The emission due to the coumarin donor in complex **3** in acetonitrile (0.1 M ^{n}Bu$_4$NClO$_4$) showed a small increase in intensity, while the emission of the rhenium(I) complex acceptor was slightly reduced in intensity upon addition of Li^+ ions. The change of the emission spectrum of complex **3** upon addition of Na^+ ions was insignificant and was too small for extraction of any useful quantitative data. On the contrary, addition of Mg^{2+} ions to complex **3** in acetonitrile (0.1 M ^{n}Bu$_4$NClO$_4$) resulted in a large increase in the coumarin donor fluorescence intensity at around 422 nm, and a drop in the rhenium(I)

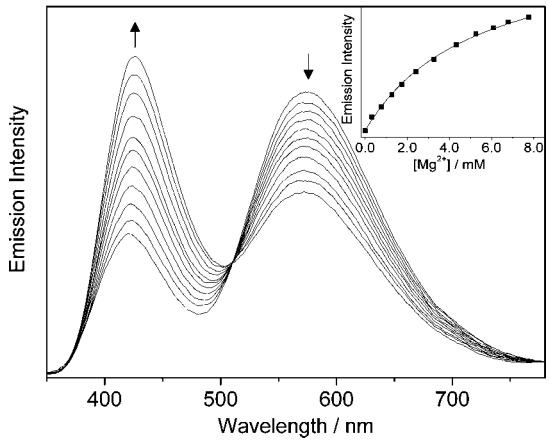

Figure 3. Emission spectral traces of $[Re(CO)_3(bpy)(\mathbf{py\text{-}O_5\text{-}CM})]^+$ (6.0×10^{-5} M) in CH_3CN (0.1 M $^n Bu_4NClO_4$) upon addition of $Mg(ClO_4)_2$. Excitation at isosbestic wavelength of 297 nm. Inset shows a plot of emission intensity at 422 nm (■) as a function of $[Mg^{2+}]$ and its theoretical fit (−) for the 1:1 binding model.

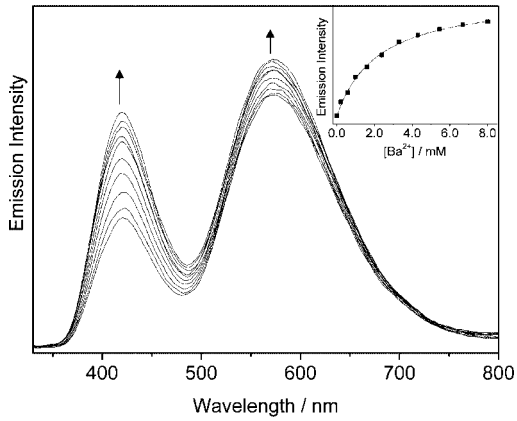

Figure 4. Emission spectral traces of $[Re(CO)_3(bpy)(\mathbf{py\text{-}O_5\text{-}CM})]^+$ (5.0×10^{-5} M) in CH_3CN (0.1 M $^n Bu_4NClO_4$) upon addition of $Ba(ClO_4)_2$. Excitation at isosbestic wavelength of 295 nm. Inset shows a plot of emission intensity at 422 nm (■) as a function of $[Ba^{2+}]$ and its theoretical fit (−) for the 1:1 binding model.

acceptor emission intensity at around 570 nm, with a perfectly clean isoemissive point at ca. 510 nm. The emission maxima of the donor moiety showed a very slight red shift upon complexation of metal ions to the oligoether chain. The emission spectral changes of complex **3** upon addition of Mg^{2+} ions and the corresponding titration curve are depicted in Figure 3. In the case of Ca^{2+} and Pb^{2+} ions, the emission of the coumarin donor also showed an increase in intensity, with a concomitant reduction in the intensity of the rhenium(I) complex acceptor emission, although the emission spectral changes were not as large as that of the Mg^{2+} ion, while for the Ba^{2+} ion, the emission of both the donor and the acceptor showed a slight increase in intensity. The emission spectral changes of complex **3** upon addition of Ba^{2+} ions and the titration curves are shown in Figure 4. The experimental data were also found to be in close agreement with the theoretical nonlinear least-squares fit to a 1:1 binding model. The binding constants were obtained and are summarized in Table 2, consistent with that determined from UV−visible spectrophotometric studies. The results showed that the binding constant of complex **3** toward Pb^{2+} was the largest and complex **3** exhibited higher binding affinity toward the alkaline earth metal ions than alkali metal ions. For the same group, the binding constants followed the order of $Ba^{2+} > Ca^{2+} > Mg^{2+}$, which has also been demonstrated using the UV−visible absorption method. Among the metal ions studied, the radius of Ba^{2+} (Ba^{2+} ∼1.36 Å, Pb^{2+} ∼1.19 Å, Ca^{2+} ∼1.00 Å, Mg^{2+} ∼0.72 Å, Na^+ ∼1.02 Å, Li^+ ∼0.76 Å)[21] was the largest and appeared to fit well in the cavity or pocket created by the oligoether chain of complex **3**. It is interesting to note that upon binding of metal ions to the oligoether chain, the FRET efficiencies, as reflected from the ratios of donor to acceptor emission intensities (I_D/I_A in Table 3), became poorer. With complex **3**, Ba^{2+} with the largest ionic radius among the group of Mg^{2+}, Ca^{2+}, and Ba^{2+} showed the least effect on the FRET efficiency upon binding, with Mg^{2+} being the smallest in size, showing the largest decrease in the FRET efficiency. It is likely that binding of the smaller metal ions would cause the largest changes in the conformation of the molecule, leading to an increase in the donor−acceptor separation that gave rise to the drop in FRET efficiency. It is also interesting to note that with Ba^{2+}, although there were changes in the I_D/I_A ratio upon binding, the overall intensities of the donor and acceptor emission were found to increase upon Ba^{2+} ion-binding. This might be ascribed to the large binding affinity of complex **3** for Ba^{2+}, which upon complexation of Ba^{2+} ion to the oxygen atoms in the oligoether chain would reduce any photoinduced electron transfer (PET) quenching of the fluorescence group by the oligoether chain, which led to the increase of the emission intensity for both the donor and acceptor moieties. The large binding constant for Ba^{2+} also implies that the ion-bound species would be most stable, causing rigidification of the molecule, and hence an increase in the emission quantum yields.

The emission properties of complex **4** upon treatment of metal ions were also studied. Emission spectral changes of complex **4** in acetonitrile similar to those of complex **3** were observed upon addition of metal ions. The binding constants of complex **4** toward different metal ions are summarized in Table 2. The binding constants of complex **4**, in general, were found to be larger than that of complexes **1**−**3** for the same metal ion, indicating that the longer oligoether chain between the donor and the acceptor showed a better binding affinity toward the metal ions, similar to results obtained from UV−visible spectrophotometric studies. Mg^{2+} ions were found to cause the most dramatic emission spectral changes in complex **4**. The emission spectral traces of complex **4** upon addition of magnesium perchlorate and the change of emission intensity at 422 nm as a function of the added metal ion concentration are shown in Figure 5. The coumarin donor emission at ca. 422 nm was enhanced by about 2-fold, and the emission of the acceptor at ca. 575 nm was quenched by ca. 50%, with a large change in the I_D/I_A ratio. Unlike complex **3**, where Pb^{2+} gave the smallest perturbation in the FRET efficiency, Ba^{2+} ion-binding gave the least perturbation in the FRET efficiency in complex **4**. It is likely that the binding of Ba^{2+} would give rise to the least changes in the donor−acceptor separation distance as a result of the best fit of Ba^{2+}, which has a slightly larger ionic radius than Pb^{2+}, to the pocket created by the slightly longer oligoether chain in complex **3**. Again, Mg^{2+} ion being smallest would give rise to the largest decrease in the FRET efficiency with an even higher sensitivity.

NMR Studies. The ion-binding properties of complex **3** have also been probed by ^1H and ^{13}C NMR spectroscopy. The assignment of protons was based on the chemical shifts, coupling patterns, and two-dimensional [^1H] COSY spectrum, as shown in the Supporting Information (Figure S1). The ^{13}C NMR

(21) Dean, J. A.; Lange, N. A. *Lange's Handbook of Chemistry*; McGraw-Hill: New York, 1999.

Table 3. Ratios of the Donor to Acceptor Emission Intensity of the Re(I) Complexes 3 and 4 Before and After Complexation with Metal Ions

		3			4		
metal ion	ionic radius/Å	$(I_D/I_A)_o$[a]	$(I_D/I_A)_{sat}$[b]	$((I_D/I_A)_{sat})/((I_D/I_A)_o)$	$(I_D/I_A)_o$[a]	$(I_D/I_A)_{sat}$[b]	$((I_D/I_A)_{sat})/((I_D/I_A)_o)$
Li^+	0.76	0.52	0.70	1.35	0.53	0.76	1.43
Na^+	1.02	0.52	0.54	1.04	0.57	0.67	1.17
Mg^{2+}	0.72	0.51	1.68	3.29	0.57	2.95	5.17
Ca^{2+}	1.00	0.49	1.18	2.41	0.55	1.09	1.99
Ba^{2+}	1.35	0.51	0.75	1.47	0.56	0.64	1.15
Pb^{2+}	1.19	0.52	0.74	1.42	0.56	0.83	1.49

[a] $(I_D/I_A)_o$ was the ratio of the donor to acceptor emission intensities of the complex before complexation with metal ions. [b] $(I_D/I_A)_{sat}$ was the ratio of the donor to acceptor emission intensities of the complex at the saturated complexation with metal ions.

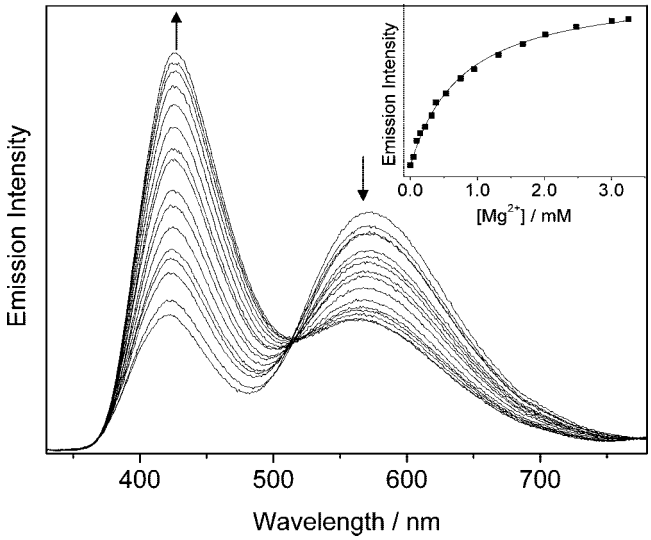

Figure 5. Emission spectral traces of $[Re(CO)_3(bpy)(\mathbf{py\text{-}O_6\text{-}CM})]^+$ (5.0×10^{-5} M) in CH_3CN (0.1 M $^n Bu_4NClO_4$) upon addition of $Mg(ClO_4)_2$. Excitation at isosbestic wavelength of 297 nm. Inset shows a plot of emission intensity at 426 nm (■) as a function of $[Mg^{2+}]$ and its theoretical fit (−) for the 1:1 binding of $[Re(CO)_3(bpy)(\mathbf{py\text{-}O_6\text{-}CM})]^+$ with metal ion in CH_3CN (0.1 M $^n Bu_4NClO_4$).

spectral assignment was obtained from [^{1}H−^{13}C] HETCOR and HMBC measurements, which are available in the Supporting Information (Figures S2 and S3). The [^{1}H−^{13}C] HETCOR and HMBC spectra of complex **3** after addition of Mg^{2+} and Ba^{2+} ions are also shown in Figures S4−S7. Large changes in the chemical shifts of complex **3** were observed in the ^{1}H NMR spectra after addition of the selected Mg^{2+} and Ba^{2+} ions as shown in Figure 6. Upon addition of the metal ions, the complexation between the complex and the metal ions would decrease the electron density at the O atoms, hence weakening the shielding effect on the neighboring protons and causing a downfield shift of the signal. A shift of proton signals for the protons in the oligoether chain, especially for those methylene protons (−CH_2−) near coumarin, was observed upon addition of Mg^{2+} ions. The signal at δ 4.38 ppm that corresponds to the −CH_2− adjacent to the coumarin unit was shifted to δ 4.61 ppm with a downfield shift ($\Delta\delta$) of ca. 0.23 ppm, while the protons of −CH_2O− adjacent to the pyridine ring did not show significant shifts by the binding interaction, indicating that the O atom of the −OCH_2− unit adjacent to the pyridine ring did not bind to the Mg^{2+} ion, probably due to the small size of the Mg^{2+} ion. This is in contrast to the binding of Ba^{2+} ions in which all of the O atoms on the oligoether chain would bind. Large changes in the ^{1}H and ^{13}C NMR signals that correspond to the coumarin unit were also observed upon addition of Mg^{2+} and Ba^{2+} ions to complex **3** (Figure 7). For instance, the carbon

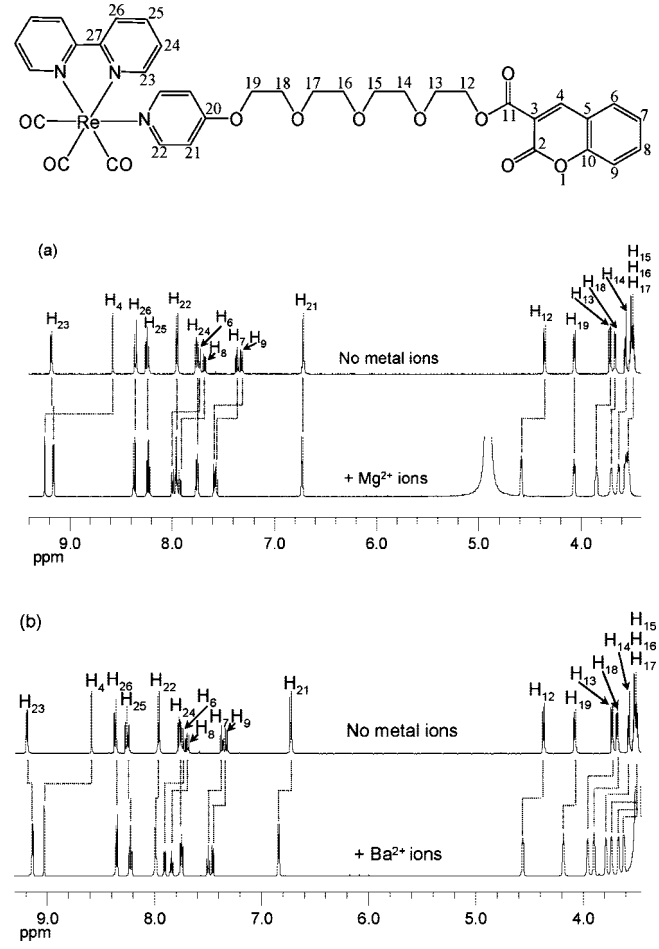

Figure 6. ^{1}H NMR spectral changes of complex **3** in CD_3CN after addition of (a) $Mg(ClO_4)_2$ and (b) $Ba(ClO_4)_2$.

signals of carbonyl groups at the 2-position and 11-position underwent a downfield shift of ca. 7.4 and 4.5 ppm after addition of Mg^{2+} ions, and ca. 3.8 and 1.5 ppm after addition of Ba^{2+} ions, respectively. The observation of larger downfield shifts of ^{13}C NMR signal at the 2-position with respect to that of 11-position upon addition of metal ions indicated that the carbonyl group at the 2-position of the coumarin unit was involved in the binding of metal ions. The strong binding interactions between the oligoether and the metal ions could lead to a large separation between coumarin and the rhenium(I) chromophore and subsequently alter the energy transfer efficiency of the complex. Control experiment was also carried out by addition of $^n Bu_4NClO_4$ to complex **3** in CD_3CN, where no changes in the proton and carbon chemical shifts were observed, further confirming that the changes in the chemical shifts of complex **3** upon addition of metal ions were a result of the binding

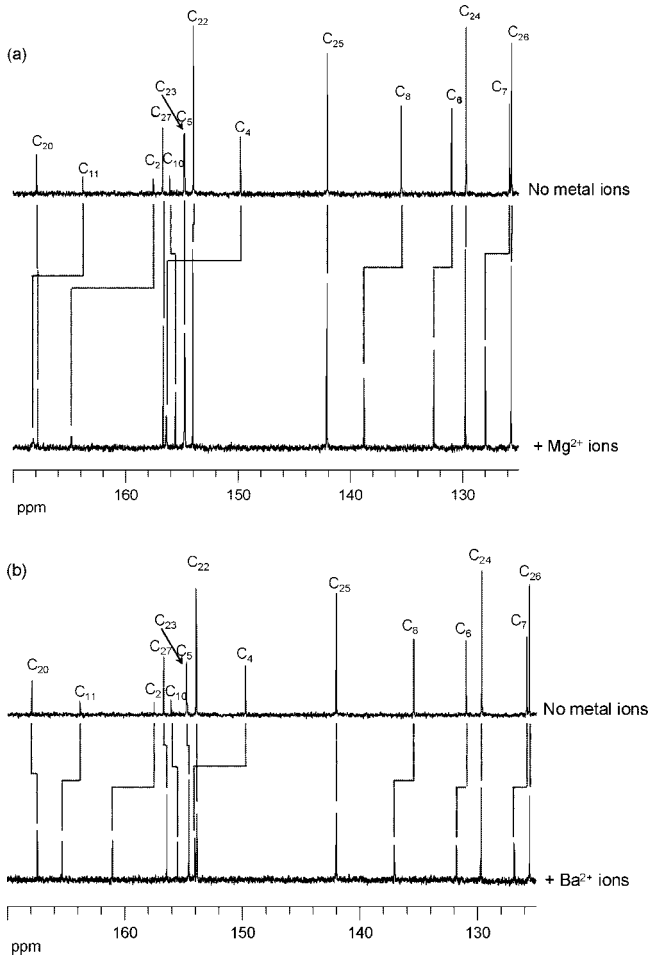

Figure 7. ^{13}C NMR spectral changes of complex **3** in CD_3CN after addition of (a) $Mg(ClO_4)_2$ and (b) $Ba(ClO_4)_2$.

interaction between the complex and the metal ions.

Transient Absorption Studies. Ultrafast absorption spectroscopy has been commonly employed in the study of energy and electron transfer processes, including those of related coumarin systems.[22] Thus, to provide further insights into the energy transfer behavior of **3** in acetonitrile, transient absorption spectroscopy of **3** on the pico- to nanosecond time scale after femtosecond laser excitation at 266 nm was carried out. For comparison purposes, parallel transient absorption measurements were also performed for coumarin-3-carboxylic acid ethyl ester and $[Re(bpy)(CO)_3py]PF_6$ in the same solvent. The transient absorption spectra of coumarin-3-carboxylic acid ethyl ester in acetonitrile recorded at various delay times are displayed in Figure 8, and the absorption time profiles at selected wavelengths are also shown. Immediately after laser excitation, an intense absorption band at 360 nm and a broad absorption at 530 nm evolved. At early picosecond times (before 15 ps, as shown in Figure 8a), the intense 360 nm band underwent fast decay accompanied by narrowing of bandwidths for both the 360 and 530 nm absorption bands. This is followed by a slower process on time scale of 15−1000 ps indicated by generation of two new bands at ~425 and ~450 nm at the expense of the decay of the 530 nm band (Figure 8b). The observation of well-

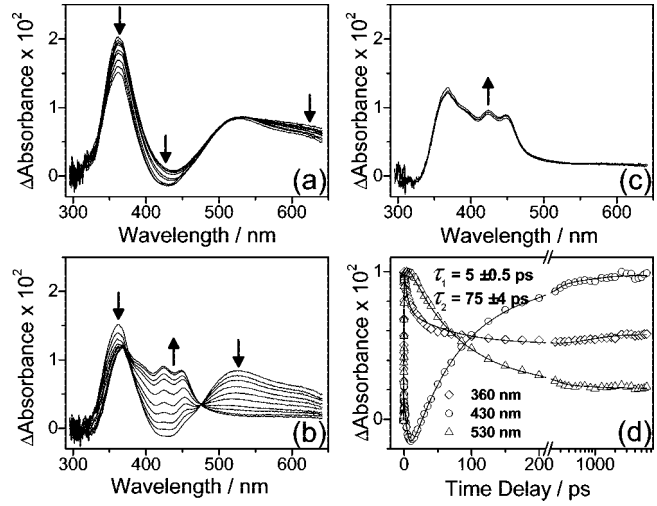

Figure 8. Transient absorption spectra of coumarin-3-carboxlic acid ethyl ester in MeCN obtained with 266 nm excitation at a series of pump−probe delays: (a) 0.4, 0.7, 1.0, 1.5, 2.5, 4.0, 7.0, 10.0, and 15.0 ps; (b) 15, 25, 35, 50, 70, 100, 150, 200, 350, and 1000 ps; (c) 1000, 2000, and 6000 ps. Part (d) shows absorption−time profiles at 360, 430, and 530 nm. The solid lines represent the IRF convoluted exponential function fitting to the experimental data. The data with time delays before and after 200 ps are displayed, respectively, on a linear and logarithmic time axis.

defined isosbestic points at ~475 and ~370 nm (Figure 8b) demonstrates a mother-to-daughter transformation from one to the second transient state associated with the spectral evolution. From Figure 8c, it can be seen that the transient spectrum associated with the second state (represented by the 1000 ps spectrum in Figure 8b) shows little change from 1000 to 6000 ps, indicating the long-lived nature of this state. Dynamics analysis on time dependences of absorption changes at representative wavelengths 360, 430, and 530 nm convolved with instrumental response function (IRF) of the transient absorption measurement resulted in a time-constant of ~5 ps for the early time process and a time-constant of 75 ps for the latter spectral conversion (Figure 8d). We note that the spectral feature of the second state (the 1000 ps spectrum in Figure 8b and the spectra in Figure 8c) resembles closely to that of the triplet (T_1) absorption spectrum of the related compound coumarin-3-carboxylic acid,[23] while the absorption spectrum of the precursor state (the 15 ps spectrum in Figure 8a and b) exhibits a feature similar to that of the singlet (S_1) absorption of coumarin-3-carboxylic acid. From this, it appears straightforward to associate the 75 ps spectral transformation to an intersystem crossing (ISC) conversion, as the precursor and product spectra have been ascribed, respectively, to the S_1 singlet and T_1 triplet state of the coumarin. As a result of this and considering that the 266 nm excitation wavelength leads to a higher singlet (S_n with $n > 1$) excitation and introduction of a significant amount of excess energy, it is reasonable to attribute the observed ~5 ps spectral evolution to the combined process of S_n to S_1 conversion and vibrational cooling of the S_1 state.

The transient absorption spectra of **3** in acetonitrile recorded at various delay times are displayed in Figure 9. At early stage after the 266 nm laser excitation of **3**, broad absorptions covering ~320 nm to and beyond 650 nm with a ~370 nm (λ_{max}) band (the 0.4 ps spectrum in Figure 9a) were observed. As time evolves, the ~370 nm band grows in on tens of picosecond

(22) (a) Okazaki, T.; Hirota, N.; Nagata, T.; Osuka, A.; Terazima, M. *J. Phys. Chem. A* **1999**, *103*, 9591. (b) Ramsteiner, I. B.; Hartschuh, A.; Port, H. *Chem. Phys. Lett.* **2001**, *343*, 83. (c) Nad, S.; Pal, H. *J. Photochem. Photobiol., A* **2000**, *134*, 9. (d) Ramakrishna, G.; Ghosh, H. N. *J. Phys. Chem. A* **2002**, *106*, 2545.

(23) Polyansky, D. E.; Neckers, D. C. *J. Phys. Chem. A* **2005**, *109*, 2793.

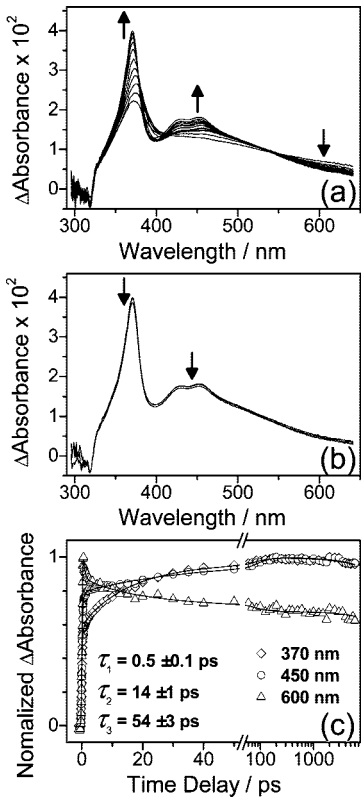

Figure 9. Transient absorption spectra of **3** in MeCN obtained with 266 nm excitation at a series of pump−probe delays: (a) 0.4, 1.0, 2.5, 5.0, 8.5, 15, 25, 35, 50, 70, 100, and 200 ps; (b) 200, 1000, and 6000 ps. Part (c) shows absorption−time profiles at 370, 450, and 600 nm. The solid lines represent the IRF convoluted exponential function fitting to the experimental data. The data with time delays before and after 50 ps are displayed, respectively, on a linear and logarithmic time axis.

time scale, and then two new bands at ∼425 and ∼450 nm develop later within 200 ps (Figure 9a). After 200 ps, the absorption profile shows little change up to 6000 ps (Figure 9b). Dynamics fitting of temporal change of the transient absorption at representative wavelengths convolved with the IRF presented three time-constants of ∼0.5, 14, and 54 ps (Figure 9c). The latter two time-constants correspond to dynamics of the ∼370 nm band growth-in and development of the ∼425 and ∼450 nm absorption, respectively. Based on comparison with the transient absorption result of $[Re(bpy)(CO)_3py]PF_6$ (Figure S8), the rapid 0.5 ps dynamics was attributed to a convoluted process of the internal conversion from the 266 nm photoexcited ^{1}IL to the ^{1}MLCT and the ISC from the ^{1}MLCT to ^{3}MLCT state of the $[Re(bpy)(CO)_3py]^+$ moiety in **3**; the following 14 ps process was ascribed to the cooling of the promptly formed vibrationally hot ^{3}MLCT excited state to its relaxed state. We note that, for Re(I) diimine tricarbonyl complexes of the type $[Re(bpy)(CO)_3(L)]^+$, the axial ligand L may influence the electronic properties and energy structures of the low-lying excited states, and hence the correlated spectroscopic features and photophysical and photochemical processes.[17,24] For the $[Re(bpy)(CO)_3py]^+$ here, previous works of the experimental[24a,b] and theoretical[24c] studies have revealed the MLCT character for both the lowest singlet excited state and the emitting triplet state. Being consistent with and to support the rapid ISC dynamics (∼0.5 ps), it is essential to mention that a subpicosecond ISC from the ^{1}MLCT to ^{3}MLCT (with time-constant of ∼0.8 ps) has been observed directly by Kerr gated time-resolved emission measurement of a closely related photochromic Re(I) tricarbonyl complex,[24d] and a femtosecond ^{1}MLCT to ^{3}MLCT ISC has been reported for the $[Re(bpy)(CO)_3Cl]$ and $[Re(bpy)(CO)_3(Etpy)]^+$ analogues.[24a] The ascription of the later ∼14 ps process to the vibrational cooling of the hot ^{3}MLCT is corroborated by the combined time-resolved UV−vis, time-resolved IR, and time-resolved resonance Raman study on the $[Re(bpy)(CO)_3Cl]$ and $[Re(bpy)(CO)_3(Etpy)]^+$ complexes.[24a] As compared to the transient spectra of $[Re(bpy)(CO)_3py]PF_6$, the two bands at ∼425 and ∼450 nm and the associated 54 ps dynamics are obviously new features that appear only for **3**. Considering that the two bands are characteristic of the T_1 absorption of coumarin (Figure 8b and c), the bands can be attributed to originate from the T_1 excited state of coumarin moiety in **3**. The spectra observed for **3** (Figure 9a and b) thus reflect combined contributions from the absorption of the $[Re(bpy)(CO)_3py]^+$ and coumarin moieties as well as perturbation introduced by the oligoether spacer. The predominance of the $[Re(bpy)(CO)_3py]^+$ absorption features over the absorption associated with coumarin excited state is due to the fact that the 266 nm excitation of **3** leads to mainly the photoexcitation of the $[Re(bpy)(CO)_3py]^+$ chromophore and a much less extent of excitation of the coumarin moieties in **3**. It is remarkable that the 54 ps coumarin T_1 formation time, that is, coumarin S_1 decay or say the coumarin ISC, in **3**, is apparently shorter than the 75 ps corresponding time observed for the free coumarin compound. This shortening of the coumarin S_1 lifetime in complex **3** indicates accessibility of an additional deactivation channel due to the presence of the oligoether-appended $[Re(bpy)(CO)_3py]^+$ complex. From this and taking into account the result of emission study described above, this additional channel may be attributed to energy transfer quenching of the coumarin S_1 by the rhenium(I) complex moiety. On the basis of these results, the energy transfer efficiency was determined to be 0.28 using the equation:[25]

$$\varphi_{ET} = 1 - \tau/\tau_o$$

Thus, upon excitation of the coumarin donor, the excited-state energy of coumarin was transferred to the rhenium(I) complex acceptor moiety with the ratio of donor to acceptor emission peak area $(I_D/I_A)_o$ of ca. 0.62. Upon addition of $Mg(ClO_4)_2$ to complex **3**, the ratio of donor to acceptor emission peak area at saturated complexation $(I_D/I_A)_{sat}$ changed to ca. 1.96, indicative of a decrease in the energy transfer efficiency. These results further demonstrated that Mg^{2+} ions would induce a poorer energy transfer efficiency, probably as a result of an increase in the separation between the donor and the acceptor moieties.

Conclusion

A series of rhenium(I) complexes with appended coumarin ligands has been synthesized and characterized, and their photophysics were studied. Obvious changes in both the UV−vis

(24) (a) Liard, D. J.; Busby, M.; Matousek, P.; Towrie, M.; Vlèek, A., Jr. *J. Phys. Chem. A* **2004**, *108*, 2363. (b) Kirgan, R. A.; Sullivan, B. P.; Rillema, D. P. *Top. Curr. Chem.* **2007**, *281*, 45. (c) Stoyanov, S. R.; Villegas, J. M.; Cruz, A. J.; Lockyear, L. L.; Reibenspies, J. H.; Rillema, D. P. *J. Chem. Theory Comput.* **2005**, *1*, 95. (d) Ko, C. C.; Kwok, W. M.; Yam, V. W. W.; Phillips, D. L. *Chem.-Eur. J.* **2006**, *12*, 5840. (e) Vlèek, A., Jr.; Busby, M *Coord. Chem. Rev.* **2006**, *250*, 1755.

(25) Attempts to determine the energy transfer efficiency of the complex from the ratio of the emission peak areas gave results with relatively large uncertainties, as both the coumarin and the rhenium(I) diimine moieties would be excited at the excitation wavelength of 297 nm.

and the emission spectra were observed upon addition of alkaline earth metal ions to a solution of the complex in CH_3CN (0.1 M $^nBu_4NClO_4$). Energy transfer efficiency from the coumarin donor to the rhenium(I) complex acceptor was also found to be perturbed upon addition of selected metal ions. The emission intensity of the coumarin donor of the complexes in acetonitrile (0.1 M $^nBu_4NClO_4$) was found to increase, while that of the rhenium(I) complex acceptor showed a decrease upon addition of Mg^{2+} ions with a drop in FRET efficiency. This has been ascribed to a change in the conformation of the molecule upon Mg^{2+} ion-binding that led to an increase in the donor−acceptor distance.

Acknowledgment. V.W.-W.Y. acknowledges support from The University of Hong Kong under the Distinguished Research Achievement Award Scheme. M.-J.L. acknowledges the receipt of a Postgraduate Studentship, and W.H.L. and C.-H.T. acknowledge the receipt of University Postdoctoral Fellowship, both from The University of Hong Kong. Miss X. Guan was acknowledged for her discussions on this manuscript. This work has been supported by a grant from the National Natural Science Foundation of China and the Research Grants Council of Hong Kong Joint Research Scheme (NSFC-RGC project No. N_HKU 737/06).

Supporting Information Available: Two-dimensional NMR spectra of **3** before and after addition of metal salts, transient absorption spectra of $[Re(bpy)(CO)_3py]PF_6$ in MeCN, and text giving the computational details, the optimized geometry of one of the possible folded conformations in **3**, and a table of the corresponding Cartesian coordinates. This material is available free of charge via the Internet http://pubs.acs.org.

OM8006486